

Regular Article

Highlighted Paper selected by Editor-in-Chief

Effective Anticancer Therapy by Combination of Nanoparticles Encapsulating Chemotherapeutic Agents and Weak Electric Current

Anowara Khatun,^a Mahadi Hasan,^{a,b†} Mahran Mohamed Abd El-Emam,^{c,d} Tatsuya Fukuta,^{a,e} Miyuki Mimura,^f Riho Tashima,^f Shintaro Yoneda,^c Shintaro Yoshimi,^f and Kentaro Kogure^{*a}

^a Graduate School of Biomedical Sciences, Tokushima University; 1–78–1 Shomachi, Tokushima 770–8505, Japan:

^b Tokyo Biochemical Research Foundation; Tokyo 103–0023, Japan: ^c Graduate School of Pharmaceutical Sciences, Tokushima University; 1–78–1 Shomachi, Tokushima 770–8505, Japan: ^d Department of Biochemistry, Faculty of Veterinary Medicine, Zagazig University; El-Shohada, Moawwad, Qesm Awel AZ, Zagazig 44511, Egypt: ^e School of Pharmaceutical Sciences, Wakayama Medical University; 25–1 Shichiban-cho, Wakayama 640–8156, Japan: and

^f Faculty of Pharmaceutical Sciences, Tokushima University; 1–78–1 Shomachi, Tokushima 770–8505, Japan.

Received August 21, 2021; accepted November 17, 2021

Delivery of medicines using nanoparticles *via* the enhanced permeability and retention (EPR) effect is a common strategy for anticancer chemotherapy. However, the extensive heterogeneity of tumors affects the applicability of the EPR effect, which needs to overcome for effective anticancer therapy. Previously, we succeeded in the noninvasive transdermal delivery of nanoparticles by weak electric current (WEC) and confirmed that WEC regulates the intercellular junctions in the skin by activating cell signaling pathways (*J. Biol. Chem.*, 289, 2014, Hama *et al.*). In this study, we applied WEC to tumors and investigated the EPR effect with polyethylene glycol (PEG)-modified doxorubicin (DOX) encapsulated nanoparticles (DOX-NP) administered *via* intravenous injection into melanoma-bearing mice. The application of WEC resulted in a 2.3-fold higher intratumor accumulation of nanoparticles. WEC decreased the amount of connexin 43 in tumors while increasing its phosphorylation; therefore, the enhancing of intratumor delivery of DOX-NP is likely due to the opening of gap junctions. Furthermore, WEC combined with DOX-NP induced a significant suppression of tumor growth, which was stronger than with DOX-NP alone. In addition, WEC alone showed tumor growth inhibition, although it was not significant compared with non-treated group. These results are the first to demonstrate that effective anticancer therapy by combination of nanoparticles encapsulating chemotherapeutic agents and WEC.

Key words weak electric current; enhanced permeability and retention effect; nanoparticle; anticancer therapy

INTRODUCTION

The microenvironment of solid tumors is characterized by a leaky and loosely compacted vasculature with poor lymphatic drainage. Intravenously administered nano-sized agents, such as liposomes, micelles, polymeric conjugates, macromolecular drugs, and imaging agents, preferentially enter the interstitial space of tumors through leaky blood vessels and are retained there. This phenomenon is known as the enhanced permeability and retention (EPR) effect.¹⁾ Currently, the passive targeting of tumor using nanoparticles *via* EPR effect is the major strategy for anticancer therapy.

The therapeutic efficacy of nanoparticles encapsulating chemotherapeutic agents following passive targeting is hampered because of the significant heterogeneity of the EPR effect.²⁾ Tumors exhibit a variety of shapes, sizes, cell densities, microenvironments, and developmental stages. Their variable endothelial gaps, irregular blood flows, differences of stromal content, and distinct interstitial fluid pressures result in a non-uniform EPR effect.^{3,4)} For example, renal cell carcinoma, and hepatocellular carcinomas tend to have good vasculature networks that support a strong EPR effect.⁵⁾ In contrast, melanomas, pancreatic cancers, prostate cancers, and metastatic liver cancers

are hypovascularized; the consequently poor EPR effect results in the suboptimal delivery of nanoparticles into these tumors.^{6,7)}

To ameliorate the delivery efficiency of nanoparticles, several approaches for the augmentation of the EPR effect have been evaluated. These strategies include increasing of tumor blood flow by either vasoconstriction or vasodilation^{8,9)}; modulation of the tumor vasculature by application of exogenous growth factors¹⁰⁾; and changing of tumor stroma *via* enzymatic degradation of the extracellular matrix.¹¹⁾ Although these strategies improved intratumor delivery and distribution of nanoparticles, the systemic administration of these pharmacological EPR modulators may also cause the delivery of nanoparticles into the normal tissue.

To address the non-specific impacts of current EPR modulating strategies, effort to enhance the EPR effect locally within tumors have garnered significant research attention. Several strategies reported in this regard include micro- or nanobubble assisted ultrasound, radiotherapy, and hyperthermia-based augmentation of nanoparticle EPR.^{5,12,13)} These strategies have achieved success to varying degree, but they all require very sophisticated instruments. Furthermore, the application of ionizing radiation, and high intensity-ultrasound may damage the normal tissue surrounding a tumor.^{14,15)}

Here, we propose an alternative strategy, iontophoresis (IP), for the enhancement of the EPR effect. IP is a noninvasive transdermal drug delivery technology that employs weak electric current (WEC) treatment by placing electrodes on

[†] Present address: Division of Animal Disease Model, Research Center for Experimental Modeling of Human Disease, Kanazawa University; 13–1 Takara-machi, Kanazawa, Ishikawa 920–8640, Japan.

* To whom correspondence should be addressed. e-mail: kogure@tokushima-u.ac.jp

the skin surface.^{16–18} A physiologically acceptable electric current density is used in WEC treatment does not exceed 0.5 mA/cm^2 . It provides the driving force for the transdermal permeation of substances across the skin barriers.¹⁹ Although small ionic and hydrophilic molecules are preferable for WEC-based delivery, we have successfully employed WEC in the noninvasive transdermal delivery of antibodies, small interfering RNA (siRNA), cytosine-phosphate-guanine (CpG) oligo DNA, and nanoparticles-encapsulated insulin.^{20–24}

In pursuit of an understanding of the molecular mechanisms underlying WEC-mediated transdermal permeation of nanoparticles, we observed that the application of WEC activates an intracellular signaling pathway leading to the opening of the intercellular space apparatus in the skin.^{25,26} In particular, the WEC-mediated opening of gap junctions and depolymerization of F-actin associated with tight junctions dramatically altered cell–cell interactions and created a paracellular pathway that contributed to the transdermal permeation of macromolecules or nanoparticles.^{19,26} Although the cutaneous physiology is different from that of tumors, in this study we hypothesized that the application of WEC on a solid tumor may increase the EPR effect *via* dissociation of intercellular junctions. Based on the hypothesis, we evaluated the EPR effect of polyethylene glycol (PEG)-modified doxorubicin (DOX) encapsulated nanoparticles (DOX-NP), the status of gap junction expression in tumors, and the antitumor effect of DOX-NP co-administered with WEC. Taken together, this study offers a novel physical approach for the augmentation of the EPR effect and effective anticancer therapy by combination of nanoparticles and WEC.

MATERIALS AND METHODS

Materials We used C57BL/6J (5 weeks old, male) mice purchased from Japan SLC, Inc. (Shizuoka, Japan). All animal procedures in this study were conducted in compliance with Tokushima University Animal and Ethics Review Committee. B16-F1 murine melanoma cells (Dainippon Sumitomo Pharma Biomedical Co., Ltd., Osaka, Japan) were grown in 10% fetal bovine serum (FBS) supplemented Dulbecco's modified Eagle's medium (DMEM) and incubated at 37°C in a 5% CO_2 atmosphere. Extracellular matrix (ECM) gel was obtained from Sigma-Aldrich Co., Ltd. (St. Louis, MO, U.S.A.). 1,2-Distearoyl-*sn*-glycero-3-phosphoethanolamine-*N*-[amino(polyethylene glycol)-2000] (ammonium salt) (DSPE-PEG 2000) and Egg phosphatidylcholine (EPC) were collected from NOF Corporation (Tokyo, Japan). The fluorescent compound 1,1'-dioctadecyl-3,3',3'-tetramethylindocarbocyanine perchlorate (DiIc18) was purchased from Thermo Fisher Scientific (Waltham, MA, U.S.A.). DOX, as doxorubicin hydrochloride, was obtained from Nacalai Tesque, Kyoto, Japan. An anti-connexin 43 (Cx43) antibody (mouse monoclonal) was purchased from Santa Cruz Biotechnology, Inc. (Santa Cruz, CA, U.S.A.). An anti-Cx43 (phospho Ser367) antibody (rabbit polyclonal) was obtained from arigo Biolaboratories (Taiwan). A rabbit polyclonal anti-Protein Kinase C (PKC) (phospho T497) antibody, an Alexa Fluor 647 conjugated goat anti-mouse immunoglobulin G (IgG) antibody, and an Alexa Fluor 488 conjugated goat anti-rabbit IgG antibody were purchased from Abcam (Cambridge, U.K.).

Preparation of DOX-NP DOX-NP was prepared according to our previous report.²⁷ In brief, EPC/DSPE-PEG2000

(10:1 M ratio) was added in chloroform, and a thin lipid film was prepared by nitrogen gas drying. The resulting film was then hydrated with 250 mM ammonium sulfate. For fluorescent labeling of the nanoparticles, DiIc18 (1 mol% of total lipid) was used. After incubation, a freeze-thawed cycle was performed three times using a dry ice/ethanol bath followed by extrusion through 100 nm pores of polycarbonate membrane filters (Nuclepore, Cambridge, MA, U.S.A.). After adjusting the size, the nanoparticle suspension was loaded into a PD-10 column (GE Healthcare Japan, Tokyo, Japan) and eluted with phosphate-buffered saline (PBS) to eliminate the excess ammonium sulfate. Then, ultracentrifugation of nanoparticles was carried out at $112500 \times g$ for 60 min at 4°C followed by the addition of 20 mM *N*-(2-hydroxyethyl)piperazine-*N'*-2-ethanesulfonic acid (HEPES) (pH 8.8) to resuspend the nanoparticle pellet. The resulting nanoparticle suspension and a DOX solution (prepared at a concentration of 2 mg/mL in 20 mM HEPES (pH 8.8)) were then mixed together to incubate for 20 min at 37°C . Next, the free DOX was separated by ultracentrifugation, and nanoparticle encapsulating DOX was evaluated by measuring the absorbance of DOX-NP dissolved in Triton X-100 (1%) at 484 nm. The nanoparticle size, ζ -potential, and polydispersity index were measured with a Zetasizer Nano ZS (Malvern Instruments, Worcestershire, U.K.). The average particle diameter was 140.83 ± 13.30 , the ζ -potential was $-1.64 \pm 1.32 \text{ mV}$, and the polydispersity index was 0.23 ± 0.02 .

Application of WEC and Evaluation of DOX-NP Accumulation in Tumors To develop melanoma-bearing mice, a suspension of 1×10^6 B16-F1 cells and ECM gel were mixed following a ratio of 5:1 (v/v), and the cells were implanted into the left posterior flank of mice that were 5 to 6 weeks of age.²⁸ After inoculation, tumor volumes were evaluated over time following this formula: tumor volume = $0.4 \times a \times b^2$ where the tumor volume is calculated in mm^3 , *a* indicates the larger diameter in mm, *b* indicates the smaller diameter in mm. Intratumor accumulation of nanoparticles following WEC application was evaluated when the tumor volume reached approximately 500 mm^3 . Intravenous (i.v.) injection of DiIc18-labeled DOX-NP was performed 1 h before the WEC treatment. For the application of WEC, anesthesia was induced in mice by intraperitoneal administration of chloral hydrate (400 mg/kg) in PBS, and the hair covering the tumor was trimmed. Ag-AgCl electrodes (3M Health Care, Minneapolis, MN, U.S.A.) with a thin layer of PBS-soaked cotton on the adhesive surface was applied to the tumor surface. The tumor was then treated with a constant current (0.4 mA/cm^2 for 1 h) by adjusting the electrodes to an external power supply (model TCCR-3005, TTI ellebeau, Inc., Tokyo, Japan). After twenty-four hours of DOX-NP administration, tumors were collected and sized into appropriately pieces. The resulting tumor tissues were subjected to snap-frozen in optimal cutting temperature (OCT) compound in a dry-ice/ethanol bath and sectioned at $10 \mu\text{m}$ thickness with a cryostat. Next, tumor sections were stained with 4',6-diaminidino-2-phenylindole (DAPI) (Dojindo, Kumamoto, Japan) and mounted with PermaFluor Aqueous Mounting Medium (Thermo Fisher Scientific), followed by observation with an LSM700 confocal laser scanning microscope (CLSM) (Carl Zeiss, Germany). For quantitative analysis, the fluorescence intensity of tumor cross-sections was quantified using ImageJ software.

Immunohistochemical Analysis of Cx43, Phospho Cx43

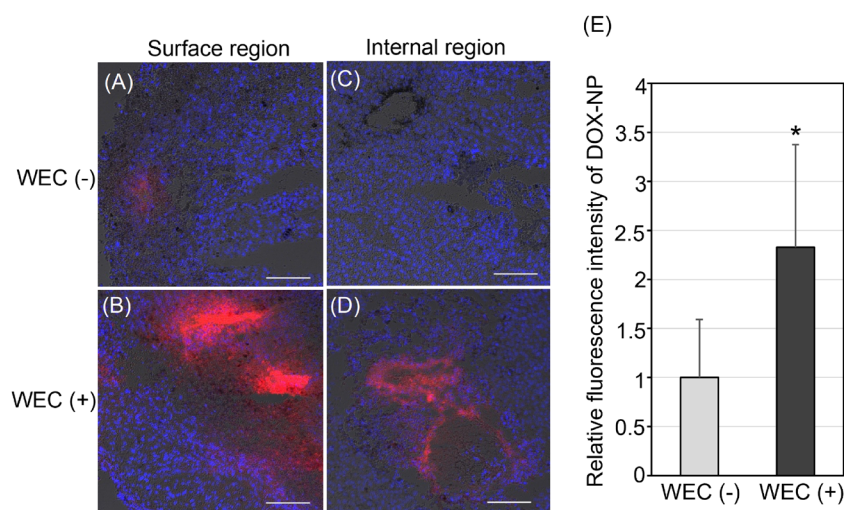


Fig. 1. Effect of WEC on Intratumor Accumulation and Distribution of DOX-NP

DiIc18-labeled DOX-NP was administered into mice bearing B16-F1 tumors *via* an IV route following application of WEC on the surface of the tumor. After 24h of WEC, tumors were collected, and their cross sections of various regions were examined with CLSM: (A) untreated surface region; (B) surface region subjected to WEC; (C) untreated internal region; (D) internal region subjected to WEC. Red indicates the accumulation of DOX-NP while blue indicates DAPI-stained nuclei. Scale bars indicate 100 μ m. (E) Quantitative analysis of DOX-NP accumulation increased by WEC. Relative fluorescence intensity of tumor sections was quantified by using image analysis software ImageJ. Data are expressed as mean \pm S.D. ($n > 3$). * $p < 0.05$.

(Ser367), and Phospho PKC (T497) in Tumor Cross-Sections after WEC Treatment

Immediately after WEC treatment as described above, tumors were harvested and 10 μ m frozen sections were generated using a cryostat. After washing with PBS (two times for 5 min) all tumor sections were blocked by PBS containing 3% bovine serum albumin (BSA) and Triton-X-100 (0.1%, 50 μ L) for 1 h at room temperature. Then, three additional washing steps were performed with PBS for 2 min and cross-sections were incubated with mouse anti-Cx43, rabbit anti-Cx43 (phospho Ser367), or rabbit anti-PKC (phospho T497) in 3% BSA/PBS at dilutions recommended by the manufacturer. After overnight incubation at 4 $^{\circ}$ C, three washing steps were carried out with PBS for 2 min, and then cross-sections were treated with an Alexa Fluor 647 conjugated anti-mouse IgG antibody or an Alexa Fluor 488 conjugated anti-rabbit IgG antibody in 3% BSA/PBS for 1 h at room temperature followed by manufacturer's instructions. Next, sections were subjected to wash again with PBS and then observed with CLSM. Fluorescence intensity of antibody staining was quantified using ImageJ software.

Investigation of the Antitumor Activity of DOX-NP in Combination with WEC After inoculation with B16-F1 cells, mice ($n = 24$) were randomly divided into four experimental groups as WEC (-) (untreated), WEC (+) (treated with WEC), DOX-NP (treated with DOX-NP), and DOX-NP + WEC (+) (treated with DOX-NP combined with WEC). IV administration of DOX-NP (3 mg DOX per kg) was started when tumor volumes reached approximately 100 mm³ and continued it on the scheduled days. After 1 h of DOX-NP administration, WEC (0.4 mA/cm² for 1 h) was applied on the tumor as described above. Over the study period, tumor volume and body weight were monitored. Mice were sacrificed at day 20 and tumors were harvested.

Statistical Analysis A one-way ANOVA followed by a Tukey *post-hoc* test was conducted for statistical analysis. Comparisons between two groups were accomplished by a Student's *t*-test. Data were representing as means \pm standard deviations (S.D.). *p*-Values < 0.05 were considered to be significant.

RESULTS AND DISCUSSION

We first examined the effect of WEC on the intratumor accumulation of DOX-NP. After IV administration of DiIc18-labeled DOX-NP into a tumor-bearing mouse, WEC was applied to the surface of the tumor. After indicated incubation time, tissue from the tumor was processed for frozen-sectioning, and then the nanoparticle accumulation into the tumor sections was observed by CLSM. From these observations, it was found that 24 h after WEC, the fluorescent signal was markedly increased in tumor tissue sections. In contrast, few fluorescent signals were observed in tissue from control tumors that did not receive WEC mentioned as WEC (-) (Fig. 1). Quantitatively, the fluorescent intensity was significantly higher in WEC-treated tumors compared to untreated control tumors (Fig. 1). These results indicate that the intratumor accumulation of nanoparticles was dramatically increased following WEC, consistent with an augmentation of the EPR effect by WEC. Additionally, we examined the effect of WEC on the pharmacokinetics (blood retention of DOX-NP) after administration of DOX-NP to normal mouse without cancer inoculation. In this experiment, we used normal mice, not tumor bearing mice, to avoid the change of pharmacokinetics of DOX-NP by enhancement of EPR effect by WEC. DOX concentrations in blood after intravenous injection of DOX-NP with or without WEC treatment were almost the same (Supplementary Fig. 1). Therefore, we concluded that WEC hardly affected the pharmacokinetics (blood retention of DOX-NP) after administration of DOX-NP.

Next, we attempted to delineate the signaling events leading to improved intratumor accumulation of nanoparticles mediated by WEC. It has been reported that WEC stimulation on the skin surface causes a transport shunt for topically applied nanoparticles or drugs into the epidermis or dermis *via* a paracellular pathway.¹⁹ This paracellular route was facilitated by WEC-mediated opening of intercellular junctions.^{19,26} Among several candidate intercellular junctions, the proteins that form gap junctions are reported to be responsive to electric stimuli.

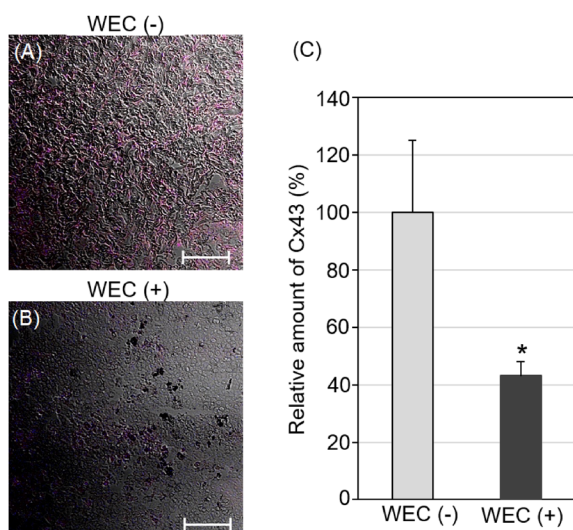


Fig. 2. Immunohistochemistry of Cx43 Expression in Tumors after WEC

Following WEC on the surface of tumor, cross sections of tumors were subjected to immunohistochemistry using an anti-Cx43 antibody and an Alexa Fluor 647 conjugated secondary antibody following observation with CLSM: (A) untreated tumor; (B) tumor subjected to WEC. Red indicates the intratumor expression of Cx43. Scale bars indicate 100 μ m. (C) Fluorescence intensity of tumor cross sections was quantified by ImageJ software. Data are expressed as mean \pm S.D. ($n > 3$). * $p < 0.05$.

For example, in the heart, gap junctions mediate rapid current transmission between adjacent cells, and they transmit presynaptic electrical currents to the postsynaptic sites in electrical synapses of neurons.^{29,30} Furthermore, increased degradation of gap junctions in diabetic retinopathy is reported to contribute to endothelial cell dysfunction and causes leakage of the blood–retinal barrier.^{31,32}

Therefore, to elucidate the mechanism of improved intratumor delivery and distribution of nanoparticles, we evaluated the expression levels and phosphorylation of the gap junction protein Cx43 in tumors following WEC. Interestingly, we found that WEC treatment significantly reduced the amount of Cx43 by approximately 57% of control levels (Fig. 2) while it increased the amount of phosphorylated Cx43 by approximately 25% of control levels (Fig. 3). As Cx43 phosphorylation is reported to attenuate gap junction assembly and to potentially induce Cx43 degradation,³³ therefore, these results are consistent with an augmentation of the EPR effect *via* WEC-mediated opening of gap junctions within the tumor microenvironment. To further investigate gap junction formation following WEC, we examined the expression and phosphorylation of PKC, which colocalizes with and directly phosphorylates Cx43.³⁴ Here, we found that phosphorylation of PKC was upregulated in the tumor immediately after application of WEC (Fig. 4). Quantitatively, the amount of phosphorylated PKC was increased by approximately 28% of control levels in WEC-treated tumors. Taken together, these results suggest that application of WEC on the tumor surface leads to activation of the signaling molecule PKC, followed by the phosphorylation of Cx43. Phosphorylated Cx43 promotes the dissociation of gap junctions and augmentation of the EPR effect. Regarding the WEC-induced change of the amount of Cx43 in the skin, it was suggested that regeneration of Cx43 protein might be occurred after decrease in the amount of Cx43 protein by enhancement of phosphorylation for recovering gap junction at 6h after iontophoresis in our previous

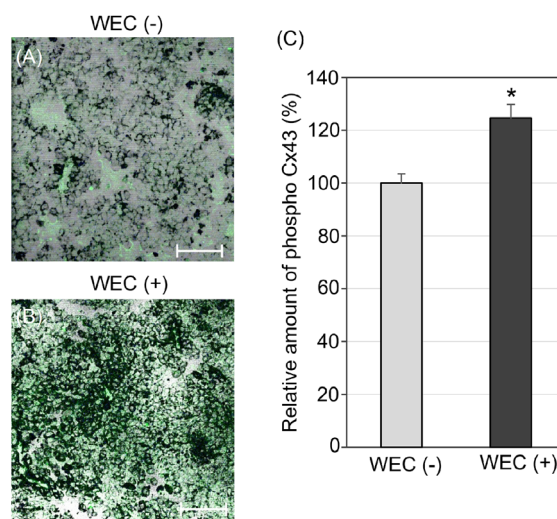


Fig. 3. Immunohistochemistry of Cx43 Phosphorylation Status in Tumors after WEC

Following application of WEC on the surface of tumor, cross sections of various regions of tumors were subjected to immunohistochemistry using an anti-Cx43 (phospho Ser367) antibody and an Alexa Fluor 488 conjugated secondary antibody followed by observation with CLSM: (A) untreated tumor; (B) tumor subjected to WEC. Green indicates the phospho-Ser367 Cx43. Scale bars indicate 100 μ m. (C) Fluorescence intensity of tumor cross sections was quantified by ImageJ software. Data are expressed as mean \pm S.D. ($n > 3$). * $p < 0.05$.

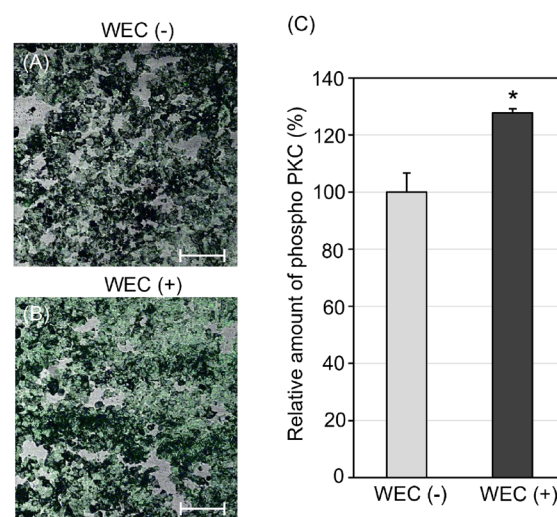


Fig. 4. Immunohistochemistry of Activation of PKC in Tumors by WEC

Following application of WEC on the tumor surface, cross sections of tumors were subjected to immunohistochemistry using an anti-PKC (phospho T497) antibody and an Alexa Fluor 488 conjugated secondary antibody, followed by observation with CLSM: (A) untreated tumor; (B) tumor subjected to WEC. Green indicates the phospho T497 PKC. Scale bars indicate 100 μ m. (C) Fluorescence intensity of tumor cross sections was quantified by ImageJ software. Data are expressed as mean \pm S.D. ($n > 3$). * $p < 0.05$.

report.²⁶) Probably, regeneration of Cx43 protein in tumor occurs approximately 6h after WEC treatment. Since the phosphorylation of PKC in tumor is a trigger event for change in intercellular junctions, this phenomenon would stop before Cx43 protein regeneration begins.

As WEC increased DOX-NP accumulation in the tumors (Fig. 1), we investigated the effect of combination of DOX-NP and WEC on tumor growth in a mouse melanoma model. DOX-NP alone showed the significant suppression of the tumor growth by 65 and 71% compared to untreated control

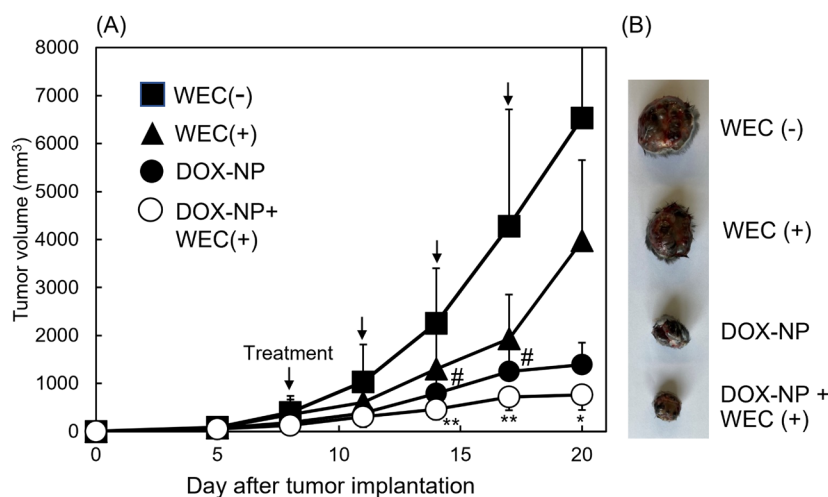


Fig. 5. Antitumor Effect of DOX-NP Combined with WEC in B16-F1 Tumor-Bearing Mice

B16-F1 cells were injected subcutaneously in C57BL/6J mice at day 0. After cells inoculation, mice ($n=24$) were randomly divided into four groups and treated with WEC/DOX-NP/DOX-NP with WEC at the indicated time point (\downarrow). The WEC (-) group did not receive any treatment. (A) Tumor growth is indicated as tumor volume measured twice in a week. Each value represents as mean \pm S.D. for six mice from each group. * $p < 0.05$, ** $p < 0.01$ vs. WEC (-) for (DOX-NP + WEC (+)); # $p < 0.05$ vs. WEC (-) for (DOX-NP). (B) Representative image of dissected tumors at day 20.

(WEC(-)) on days 14 and 17, respectively (Fig. 5). Furthermore, combination of DOX-NP with WEC(+) significantly inhibited the tumor growth by 80, 83 and 88% on days 14, 17 and 20, respectively. The tumor volumes of the group treated with the combination of DOX-NP and WEC(+) were around 43% compared to those of DOX-NP alone on day 14, 17 and 20. Thus, although DOX-NP alone also inhibited tumor growth, the combined application of DOX-NP with WEC(+) provided a more potent antitumor effect. This result is consistent with the improvement in intratumor accumulation of DOX-NP by WEC (Fig. 1). In addition, WEC treatment alone (WEC(+)) also reduced the tumor growth, although the effect of WEC(+) was not statistical significant (Fig. 5). This result suggests that weak electricity has the possibility of anticancer activity. Previously, we reported that WEC induced the upregulation and downregulation of cytoplasmic protein phosphorylation.²⁵⁾ The number of proteins showing upregulated and downregulated phosphorylation by WEC treatment was 139 and 15, respectively. The three types of acidic leucine-rich nuclear phosphoprotein 32 (ANP32A, ANP32B and ANP32E) were included in the downregulated 15 proteins. The ANP32 family protein plays an important role in the cancer cell proliferation.³⁵⁻³⁹⁾ Since the phosphorylation is required for activation of ANP32, the functionality regarding tumor growth of ANP32 would reduce *via* downregulation of protein phosphorylation by WEC treatment. Probably, the downregulation of ANP32 phosphorylation would be the reason for anticancer activity by WEC in this study. Thus, WEC would have some degree of anticancer activity, although it is not significant. Therefore, it was suggested that the potent suppression of tumor growth by the combination of DOX-NP and WEC(+) was the additive effect of two WEC effects (intratumor accumulation improvement of DOX-NP and direct anticancer activity).

In conclusion, we show for the first time that the application of WEC significantly augments the EPR effect to increase intratumor accumulation and distribution of DOX-NP, and additionally WEC has direct anticancer activity. Mechanistically, improvement of the EPR effect seems to be due to WEC-mediated activation of cell signaling and opening of gap junc-

tions in tumors, and anticancer activity would be caused by downregulation of ANP32 protein phosphorylation. Because of the augmentation of the EPR effect and direct anticancer activity by weak electricity, we propose the combination of nanoparticles encapsulating chemotherapeutic agents and WEC as the effective anticancer therapy.

Acknowledgments This work was supported by JSPS KAKENHI (Grant No. 17H03976), Tokushima University & Taiho Pharmaceutical Inc. basic research promotion council and a Tokushima University research program for the development of an intelligent Tokushima artificial exosome (iTEX).

Conflict of Interest The authors declare no conflict of interest.

Supplementary Materials This article contains supplementary materials.

REFERENCES

- 1) Matsumura Y, Maeda H. A new concept for macromolecular therapeutics in cancer chemotherapy: mechanism of tumorotropic accumulation of proteins and antitumor agent smancs. *Cancer Res.*, **46**, 6387-6392 (1986).
- 2) Maeda H. Toward a full understanding of the EPR effect in primary and metastatic tumors as well as issues related to its heterogeneity. *Adv. Drug Deliv. Rev.*, **91**, 3-6 (2015).
- 3) Rosenblum D, Joshi N, Tao W, Karp JM, Peer D. Progress and challenges towards targeted delivery of cancer therapeutics. *Nat. Commun.*, **9**, 1410 (2018).
- 4) Nakamura Y, Mochida A, Choyke PL, Kobayashi H. Nanodrug delivery: is the enhanced permeability and retention effect sufficient for curing cancer? *Bioconjug. Chem.*, **27**, 2225-2238 (2016).
- 5) Duan L, Yang L, Jin J, Yang F, Liu D, Hu K, Wang Q, Yue Y, Gu N. Micro/nano-bubble assisted ultrasound to enhance EPR effect and potential theranostic applications. *Theranostics*, **10**, 462-483 (2020).
- 6) Kinoshita R, Ishima Y, Chuang VTG, Nakamura H, Fang J, Watanabe H, Shimizu T, Okuhira K, Ishida T, Maeda H, Otagiri M,

- Maruyama T. Improved anticancer effects of albumin-bound paclitaxel nanoparticle *via* augmentation of EPR effect and albumin-protein interactions using S-nitrosated human serum albumin dimer. *Biomaterials*, **140**, 162–169 (2017).
- 7) Islam W, Fang J, Imamura T, Etrych T, Subr V, Ulbrich K, Maeda H. Augmentation of the enhanced permeability and retention effect with nitric oxide-generating agents improves the therapeutic effect of nanomedicines. *Mol. Cancer Ther.*, **17**, 2643–2653 (2018).
 - 8) Nagamitsu A, Greish K, Maeda H. Elevation blood pressure as a strategy to increase tumor targeted delivery of macromolecular drug smancs: case of advanced solid tumors. *Jpn. J. Clin. Oncol.*, **39**, 756–766 (2009).
 - 9) Tahara Y, Yoshikawa T, Sato H, Mori Y, Zahangir MH, Kishimura A, Mori T, Katayama Y. Encapsulation of a nitric oxide donor into a liposome to boost the enhanced permeation and retention (EPR) effect. *Medchemcomm*, **8**, 415–421 (2017).
 - 10) Monsky WL, Fukumura D, Gohongi T, Ancukiewicz M, Weich HA, Torchilin VP, Yuan F, Jain RK. Augmentation of transvascular transport of macromolecules and nanoparticles in tumors using vascular endothelial growth factor. *Cancer Res.*, **59**, 4129–4135 (1999).
 - 11) Magzoub M, Jin S, Verkman AS. Enhanced macromolecule diffusion deep in tumors after enzymatic digestion of extracellular matrix collagen and its associated proteoglycan decorin. *FASEB J.*, **22**, 276–284 (2008).
 - 12) Kobayashi H, Reijnders K, English S, Yordanov AT, Milenic DE, Sowers AL, Citrin D, Krishna MC, Waldmann TA, Mitchell JB, Brechbiel MW. Application of macromolecular contrast agent for detection of alteration of tumor vessel permeability induced by radiation. *Clin. Cancer Res.*, **10**, 7712–7720 (2004).
 - 13) Li L, ten Hagen TLM, Bolkestein M, Gasselhuber A, Yatvin J, van Rhoon GC, Eggermont AMM, Haemmerich D, Koning GA. Improved intratumoral nanoparticle extravasation and penetration by mild hyperthermia. *J. Control. Release*, **167**, 130–137 (2013).
 - 14) Fang J, Islam W, Maeda H. Exploiting the dynamic of the EPR effect and strategies to improve the therapeutic effects of nanomedicines by using EPR effect enhancers. *Adv. Drug Deliv. Rev.*, **157**, 142–160 (2020).
 - 15) Dhaliwal A, Zheng G. Improving accessibility of EPR-insensitive tumor phenotypes using EPR-adaptive strategies: designing a new perspective in nanomedicine delivery. *Theranostics*, **9**, 8091–8108 (2019).
 - 16) Kalia YN, Naik A, Garrison J, Guy RH. Iontophoretic drug delivery. *Adv. Drug Deliv. Rev.*, **56**, 619–658 (2004).
 - 17) Hasan M, Nishimoto A, Ohgita T, Hama S, Kashida H, Asanuma H, Kogure K. Faint electric treatment-induced rapid and efficient delivery of extraneous hydrophilic molecules into the cytoplasm. *J. Control. Release*, **228**, 20–25 (2016).
 - 18) Hasan M, Tarashima N, Fujikawa K, Ohgita T, Hama S, Tanaka T, Saito H, Minakawa N, Kogure K. The novel functional nucleic acid iRed effectively regulates target genes following cytoplasmic delivery by faint electric treatment. *Sci. Technol. Adv. Mater.*, **17**, 554–562 (2016).
 - 19) Hasan M, Khatun A, Fukuta T, Kogure K. Noninvasive transdermal delivery of liposomes by weak electric current. *Adv. Drug Deliv. Rev.*, **154–155**, 227–235 (2020).
 - 20) Fukuta T, Oshima Y, Michiue K, Tanaka D, Kogure K. Non-invasive delivery of biological macromolecular drugs into the skin by iontophoresis and its application to psoriasis treatment. *J. Control. Release*, **323**, 323–332 (2020).
 - 21) Torao T, Mimura M, Oshima Y, Fujikawa K, Hasan M, Shimokawa T, Yamazaki N, Ando H, Ishida T, Fukuta T, Tanaka T, Kogure K. Characteristics of unique endocytosis induced by weak current for cytoplasmic drug delivery. *Int. J. Pharm.*, **576**, 119010 (2020).
 - 22) Kigasawa K, Kajimoto K, Hama S, Saito A, Kanamura K, Kogure K. Noninvasive delivery of siRNA into the epidermis by iontophoresis using an atopic dermatitis-like model rat. *Int. J. Pharm.*, **383**, 157–160 (2010).
 - 23) Kigasawa K, Kajimoto K, Nakamura T, Hama S, Kanamura K, Harashima H, Kogure K. Noninvasive and efficient transdermal delivery of CpG-oligodeoxynucleotide for cancer immunotherapy. *J. Control. Release*, **150**, 256–265 (2011).
 - 24) Kajimoto K, Yamamoto M, Watanabe M, Kigasawa K, Kanamura K, Harashima H, Kogure K. Noninvasive and persistence transfollicular drug delivery system using a combination of liposomes and iontophoresis. *Int. J. Pharm.*, **403**, 57–65 (2011).
 - 25) Hasan M, Hama S, Kogure K. Low electric treatment activates Rho GTPase *via* heat shock protein 90 and protein kinase C for intracellular delivery of siRNA. *Sci. Rep.*, **9**, 4114 (2019).
 - 26) Hama S, Kimura Y, Mikami A, Shiota K, Toyoda M, Tamura A, Nagasaki Y, Kanamura K, Kajimoto K, Kogure K. Electric stimulus opens intercellular spaces in skin. *J. Biol. Chem.*, **289**, 2450–2456 (2014).
 - 27) Fukuta T, Yoshimi S, Kogure K. Leukocyte-mimetic liposomes penetrate into tumor spheroids and suppress spheroid growth by encapsulated doxorubicin. *J. Pharm. Sci.*, **110**, 1701–1709 (2021).
 - 28) Toyoda M, Hama S, Ikeda Y, Nagasaki Y, Kogure K. Anti-cancer vaccination by transdermal delivery of antigen peptide-loaded nanogels *via* iontophoresis. *Int. J. Pharm.*, **483**, 110–114 (2015).
 - 29) Epifantseva I, Shaw MR. Intracellular trafficking pathways of Cx4 gap junction channels. *Biochim. Biophys. Acta Biomembr.*, **1860**, 40–47 (2018).
 - 30) Pereda AE, Curti S, Hoge G, Cachepe R, Flores CE, Rash JE. Gap junction-mediated electrical transmission: regulatory mechanism and plasticity. *Biochim. Biophys. Acta*, **1828**, 134–146 (2013).
 - 31) Fernandes R, Girao H, Pereira P. High glucose down-regulates intracellular communication in retinal endothelial cells by enhancing degradation of connexin 43 by a proteasome-dependent mechanism. *J. Biol. Chem.*, **279**, 27219–27224 (2004).
 - 32) Bobbie MW, Roy S, Trudeau K, Munger SJ, Simon AM, Roy S. Reduction of connexin 43 expression and its effect on the development of the vascular lesions in retinas of diabetic mice. *Invest. Ophthalmol. Vis. Sci.*, **51**, 3758–3763 (2010).
 - 33) Solan JL, Lampe PD. Specific Cx43 phosphorylation events regulate gap junction turnover *in vivo*. *FEBS Lett.*, **588**, 1423–1429 (2014).
 - 34) Liu W, Cui Y, Wei J, Sun J, Zheng L, Xie J. Gap junction mediated cell to cell communication in oral development and oral disease: a concise review of research progress. *Int. J. Oral Sci.*, **12**, 17 (2020).
 - 35) Yang S, Zhou L, Reilly PT, Shen SM, He P, Zhu XN, Li CX, Wang LS, Mak TW, Chen GQ, Yu Y. ANP32B deficiency impairs proliferation and suppresses tumor progression by regulating AKT phosphorylation. *Cell Death Dis.*, **7**, e2082 (2016).
 - 36) Yan W, Bai Z, Wang J, Li X, Chi B, Chen X. ANP32A modulates cell growth by regulating p38 and Akt activity in colorectal cancer. *Oncol. Rep.*, **38**, 1605–1612 (2017).
 - 37) Huang J, Gao W, Liu H, Yin G, Duan H, Huang Z, Zhang Y. Up-regulated ANP32E promotes the thyroid carcinoma cell proliferation and migration *via* activating AKT/mTOR/HK2-mediated glycolysis. *Gene*, **750**, 144681 (2020).
 - 38) Zhang J, Lan Z, Qiu G, Ren H, Zhao Y, Gu Z, Li Z, Feng L, He J, Wang C. Over-expression of ANP32E is associated with poor prognosis of pancreatic cancer and promotes cell proliferation and migration through regulating beta-catenin. *BMC Cancer*, **20**, 1065 (2020).
 - 39) Tian Z, Liu Z, Fang X, Cao K, Zhang B, Wu R, Wen X, Wen Q, Shi H, Wang R. ANP32A promotes the proliferation, migration and invasion of hepatocellular carcinoma by modulating the HMGAI/STAT3 pathway. *Carcinogenesis*, **42**, 493–506 (2021).